

Model Predictive Idle Speed Control: Design, Analysis, and Experimental Evaluation

Stefano Di Cairano, *Member, IEEE*, Diana Yanakiev, *Member, IEEE*, Alberto Bemporad, *Fellow, IEEE*, Ilya. V. Kolmanovsky, *Fellow, IEEE*, and Davor Hrovat, *Fellow, IEEE*

Abstract—Idle speed control is a landmark application of feedback control in automotive vehicles that continues to be of significant interest to automotive industry practitioners, since improved idle performance and robustness translate into better fuel economy, emissions and drivability. In this paper, we develop a model predictive control (MPC) strategy for regulating the engine speed to the idle speed set-point by actuating the electronic throttle and the spark timing. The MPC controller coordinates the two actuators according to a specified cost function, while explicitly taking into account constraints on the control and requirements on the acceptable engine speed range, e.g., to avoid engine stalls. Following a process proposed here for the implementation of MPC in automotive applications, an MPC controller is obtained with excellent performance and robustness as demonstrated in actual vehicle tests. In particular, the MPC controller performs better than an existing baseline controller in the vehicle, is robust to changes in operating conditions, and to different types of disturbances. It is also shown that the MPC computational complexity is well within the capability of production electronic control unit and that the improved performance achieved by the MPC controller can translate into fuel economy improvements.

Index Terms—Automotive control, engine control, model predictive control (MPC), real-time control.

I. INTRODUCTION

IN recent years, the fuel economy and emissions standards for automotive vehicles grew stricter, while the competitive pressures to deliver improved fuel economy and driveability have been also increasing. With every aspect of the automotive systems being scrupulously optimized to satisfy these demands, the interest in control solutions which can improve performance and robustness with zero variable-cost has been rising. In this regard, model predictive control (MPC) [3], [4], that has been successfully applied in chemical process industry for years, is increasingly seen as an attractive technology due to its capability to directly handle various specification requirements, including the coordination of multiple actuators through the op-

timization of an appropriately defined cost function while enforcing pointwise-in-time constraints on state and control variables. Recent applications of MPC for powertrain control include control of diesel engines [5], [6], catalyst control [7], [8], transmission control [9], powertrain actuator control [10], [11], and hybrid electric powertrain energy management [12], [13]. Explicit MPC techniques [14] can be used to synthesize the controller as a piecewise affine function. With this approach appropriately applied, the MPC can be implemented in the micro-controller without the need for an optimization solver and satisfying limitations on memory and computational power characteristic of automotive electronic control units (ECUs).

In this paper, we demonstrate the design, synthesis, and in-vehicle validation of a model predictive controller for idle speed control (ISC) [15], [16]. While ISC is related to one of the oldest regulation mechanisms in history (Watt's governor, 1787), it still represents a challenging problem for industry practitioners, where improvements in performance and robustness can directly translate into better fuel economy and emissions. For instance, it is desirable to set the idle speed set-point as low as possible, since with lower idling speed, fuel consumption is reduced [15]. However, lowering idle speed increases the possibility of engine stalls, and requires the control strategy to be fast enough to counteract disturbances. An excessive reduction of idle speed may also increase noise, vibration, and harshness (NVH). While simple regulators can be implemented by PID loops or pole-placement linear controllers (see, e.g., [15]) actuating an electronic throttle (or an air bypass valve in older engines), advanced designs, based on more sophisticated control algorithms and capable of coordinating several actuators, can provide better performance.

The spark ignition timing can be used as a second actuator [17] to complement the electronic throttle. At nominal, close to steady-state conditions, the ignition timing is retarded relative to the optimal timing for minimum fuel consumption. Even though this somewhat degrades fuel economy, it also creates a torque reserve that can be quickly utilized for disturbance rejection, by changing the spark timing up to the optimal value when needed. As a consequence, the idle speed controller relies on two actuators, the throttle, with large steady-state authority and slow response (because of throttle time constant, intake-to-torque delay and manifold filling dynamics), and the spark timing, with small steady-state authority and fast response [16]. Both actuators are constrained, and obviously, if a given controller can operate with smaller spark reserve, the efficiency of the engine operation can be improved.

In this paper, we discuss the development and experimental vehicle implementation of two model predictive controllers for

Manuscript received March 30, 2010; revised October 02, 2010; accepted December 13, 2010. Manuscript received in final form January 30, 2011. Date of publication March 07, 2011; date of current version December 14, 2011. Recommended by Associate Editor J. Lu.

S. Di Cairano, D. Yanakiev, and D. Hrovat are with the Ford Research and Adv. Engineering, Dearborn, MI 48124 USA (e-mail: sdicaira@ford.com; dyanakie@ford.com; dhrovat@ford.com).

A. Bemporad is with the Department of Mechanical and Structural Engineering, University of Trento, 38100 Italy (e-mail: bemporad@ing.unitn.it).

I. V. Kolmanovsky is with the Department of Aerospace Engineering, University of Michigan, Ann Arbor, MI 48109 USA (e-mail: ilya@umich.edu).

Color versions of one or more of the figures in this paper are available online at <http://ieeexplore.ieee.org>.

Digital Object Identifier 10.1109/TCST.2011.2112361

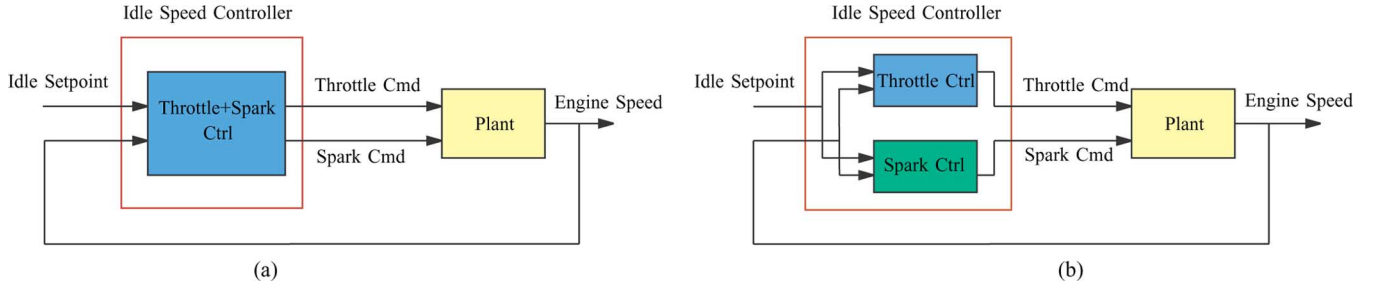


Fig. 1. Structure of the idle speed controller architectures discussed in this paper. (a) Multi-input ISC structure. The throttle and spark are controlled in a single loop, and are coordinated. (b) Single-input ISC structure. Two separated loops control the throttle and spark without coordination.

engine speed regulation. The first controller uses MPC to actuate both throttle and spark timing in a single control function, as shown in Fig. 1(a). The second controller uses MPC to actuate only the throttle, with the spark timing being conventionally controlled, hence using two separated channels as shown in Fig. 1(b). The second controller is of interest in the view of idle speed control implementation within the existing modular partitioning of the ECU software and for evaluating the performance/robustness advantages and computational disadvantages of the controller which uses two actuators over the one that uses a single actuator.

The idea of applying MPC to idle speed control was first proposed in [18], but most of the modern MPC tools which facilitate implementation and closed-loop analysis were not available at the time, hence the controller could not be implemented in real-time and tested in the vehicle. Here, explicit implementation of our MPC controllers will be demonstrated to enable their closed-loop analysis and implementation in the vehicle. Several advanced techniques have been considered in the literature for idle speed control: H_∞ [19], μ synthesis [20], neural networks [21], optimal control [22], estimator-based control [23], output feedback stabilization [24], variable structure control [17], [25], and adaptive control [26]. See also the references therein. The attractiveness of MPC over these and other approaches to idle speed control includes the capability to handle systematically a significant variety of closed-loop requirements, and to respond optimally in presence of limits on actuator ranges and engine speed range, while predictively accounting for the effects of engine dynamics and time-delay. This ensures fast recovery of engine speed in response to disturbances that cannot be easily achieved with conventional linear or robust controllers. These observations are confirmed with our vehicle tests, in which the MPC controllers exhibited excellent performance and robustness. While the computational complexity of the MPC controllers may be higher than of other control techniques, as we will demonstrate, it is well within the capability of the production ECU.

A. Design Flow

Besides treating a specific application, in this paper we propose and validate a process flow for design of MPC controllers that can be used more broadly in automotive applications. The trend in the automotive industry has been towards increasing deployment of model-based control system design paradigms, wherein plant models based on first principles and system

identification are used to facilitate the design, tuning, analysis and validation of the control system. Model-based development framework facilitates controller implementation through auto-coding. With model-based design, the time, effort, and cost for control design, calibration, and testing can be reduced, eventually allowing simultaneous releases of control algorithms software and calibrations along with hardware.

The design flow of MPC controllers, which we have used for the idle speed control problem and believe has broader applicability, is synergistic with the model-based development framework. It is composed of the following steps.

- 1) Based on first principle modeling and already available experimental data (if any), a full simulation model of the system is developed, along with a simpler control-oriented model, which is sufficiently representative to be used as the MPC prediction model. The model type and order of the control-oriented model are design parameters selected at this stage. This step is discussed in Section II.
- 2) The MPC controller is designed by augmenting the control-oriented model with additional states to enforce specifications, and by defining the appropriate cost function and constraints. The cost function weights and the prediction horizon (the number of integration steps) are the design parameters selected at this stage. The obtained controller is simulated in closed-loop with the full simulation model to evaluate the performance and the relation between closed-loop performance and tuning parameters. This step is discussed in Section III.
- 3) The MPC controller is synthesized in a suitable way for implementation in automotive ECUs. We use the explicit form of the MPC that allows also to assess closed-loop asymptotic stability and CPU and memory load. The complexity of the explicit MPC controller depends on the number of constraints and on the number of the degrees of freedom that can be tuned by selecting the constraint and control horizons. Once the computational feasibility of the controller is verified along with its simulated performance, experimental data from the target vehicle can be obtained, to update the model parameters for the specific application. This step is discussed in Section IV.
- 4) Experimental tests are performed to validate the nominal and non-nominal performance of the closed-loop system, as illustrated in Section V.

These steps are now discussed in detail, while concluding remarks are reported in Section VI.

II. ENGINE MODEL FOR IDLE SPEED CONTROL

The relevant engine dynamics for the idle speed control problem are the torque production and the crankshaft rotational dynamics. The engine crankshaft rotational dynamics are described by Newton's second law

$$\dot{N}(t) = \frac{1}{J} \frac{30}{\pi} (M_e(t) - M_L(t)) \quad (1)$$

where N [RPM] is the engine speed, M_e [Nm] is the net engine torque (engine brake torque), and M_L [Nm] is the load torque on the crankshaft.

In port-fuel injection engines, the torque cannot be changed instantaneously [15], and engine torque production dynamics have to be considered

$$M_e(t) = \kappa_{\text{spk}}(t - t_{ds})M_{e,\delta}(t - t_d) - M_{\text{fr}}(t) - M_{\text{pmp}}(t) \quad (2)$$

where $M_{e,\delta}(t - t_d)$ [Nm] is the indicated torque delayed by the intake-to-torque production time delay, t_d [s], $M_{\text{fr}}(t)$ [Nm] is the engine friction torque loss, and $M_{\text{pmp}}(t)$ [Nm] is the pumping torque loss. The torque ratio κ_{spk} , subject to the (constant) actuation delay t_{ds} , is function of the spark ignition angle α [rad] and of the maximum brake torque ignition angle α_{MBT} [rad], in radians before top dead center (TDC)

$$\kappa_{\text{spk}}(t) = f_{\text{spk}}(\alpha(t), \alpha_{\text{MBT}}(t)). \quad (3)$$

For instance, in [17] the following form for f_{spk} is suggested:

$$f_{\text{spk}}(\alpha, \alpha_{\text{MBT}}) = (\cos(\alpha - \alpha_{\text{MBT}}))^{\xi} \quad (4)$$

where $\xi \in [2.5, 3]$ is an engine dependent constant parameter, and α is bounded, $\alpha \in [\underline{\alpha}, \bar{\alpha}]$. The MBT angle α_{MBT} is function of engine speed and of the (mean) mass flow rate into the engine cylinders W_{cyl} [kg/s]

$$\alpha_{\text{MBT}} = f_{\text{MBT}}(W_{\text{cyl}}, N). \quad (5)$$

Function f_{MBT} is obtained from engine mapping. In general, f_{MBT} decreases with N and increases with W_{cyl} . We do not consider the dependence of α_{MBT} on other variables, such as cam timing, given our interest in the model for near idle operating conditions.

In (2), t_d is about 360 degrees of the crankshaft revolution

$$t_d(t) = \frac{60}{N(t)}. \quad (6)$$

Additional dynamics are associated with manifold filling. Under constant manifold gas temperature, the intake manifold pressure dynamics are

$$\dot{p}_{\text{im}} = \frac{RT_{\text{im}}}{V_{\text{im}}}(W_{\text{th}} - W_{\text{cyl}}) \quad (7)$$

where W_{th} [kg/s] is the mass flow rate through the electronic throttle. In (7), T_{im} [K] is the intake manifold temperature, V_{im} [m³] is the intake manifold volume and R is the ideal gas constant in kJ/kg/K. Although constant manifold gas temperature is a reasonable approximation at this stage, further refinements are possible by relaxing this assumption [27], which can be considered for future work. Assuming

stoichiometric air-to-fuel ratio, the indicated engine torque is approximately proportional to the cylinder air charge m_{cyl} [kg]

$$M_{e,\delta}(t) = \gamma_1 m_{\text{cyl}}(t) = \gamma_1 \frac{W_{\text{cyl}}(t)}{N(t)} \quad (8)$$

where γ_1 is an engine-speed dependent parameter. The cylinder flow is a function of the intake manifold pressure p_{im} [Pa] and engine speed N

$$W_{\text{cyl}}(t) = \frac{\gamma_2}{\gamma_1} p_{\text{im}}(t)N(t) + \gamma_0 \quad (9)$$

and γ_0 , γ_2 are constant parameters. Near idle, the flow through the throttle is choked and one can approximate

$$W_{\text{th}}(t) = \gamma_3 \vartheta(t) \quad (10)$$

where ϑ [deg] is the throttle position and γ_3 is an engine dependent constant. From (8) and (9) it follows that $M_{e,\delta}(t) = \gamma_2 p_{\text{im}}(t) + (\gamma_1/N(t))\gamma_0$. Differentiating this and using (7), (9), and (10)

$$\dot{M}_{e,\delta} = -\gamma_2 \frac{RT_{\text{im}}}{V_{\text{im}}} \frac{N}{\gamma_1} M_{e,\delta} + \gamma_2 \frac{RT_{\text{im}}}{V_{\text{im}}} \gamma_3 \dot{\vartheta} - \frac{\gamma_0 \cdot \gamma_1}{N^2} \dot{N}. \quad (11)$$

Thus, the complete engine model near idle is

$$\dot{N}(t) = \frac{1}{J} \frac{30}{\pi} (M_e(t) - M_L(t)) \quad (12a)$$

$$M_e(t) = \kappa_{\text{spk}}(t - t_{ds})M_{e,\delta}(t - t_d) - M_{\text{fr}}(t) - M_{\text{pmp}}(t) \quad (12b)$$

$$\kappa_{\text{spk}}(t) = (\cos(\alpha(t) - \alpha_{\text{MBT}}(t)))^{\xi} \quad (12c)$$

$$t_d(t) = \frac{60}{N(t)} \quad (12d)$$

$$\begin{aligned} \dot{M}_{e,\delta}(t) = & -\gamma_2 \frac{RT_{\text{im}}}{V_{\text{im}}} \frac{N(t)}{\gamma_1} M_{e,\delta}(t) + \gamma_2 \frac{RT_{\text{im}}}{V_{\text{im}}} \gamma_3 \dot{\vartheta}(t) \\ & - \frac{\gamma_0 \cdot \gamma_1}{N^2} \dot{N}(t) \end{aligned} \quad (12e)$$

where M_{fr} , M_{pmp} , M_L , α_{MBT} , ϑ , and α are independent variables.

A. Control Oriented Models

Starting from the complete model (12) we obtain a simplified control-oriented model for MPC predictions. The model order affects the complexity of the MPC controller, hence we look for the smallest order which represents the relevant dynamics. To simplify the model and remove the nonlinearity in (12c), we use the torque ratio κ_{spk} as a control variable. The spark ignition angle α is generated by inverting (4) for the current value α_{MBT} , obtained evaluating (5) at the current operating conditions and subject to the condition $\alpha \leq \alpha_{\text{MBT}}$. As a result, the control inputs are the throttle position ϑ and the torque ratio achieved via spark retard κ_{spk} . The torque pumping losses, friction, and loads are seen as disturbances, and their nominal values are compensated by feedforward.

Since the idle speed controller will operate for most of the time in a limited speed and torque range, (12) can be linearized without introducing excessive modeling errors. Let \bar{N} , be the nominal idle speed, $\bar{\kappa}_{\text{spk}}$ be the desired nominal torque ratio at idle, \bar{M}_e the nominal engine torque at idle, obtained by applying the nominal idle throttle position $\bar{\vartheta}$. \bar{M}_e , $\bar{\vartheta}$, and $\bar{\kappa}_{\text{spk}}$ are such

that the system is at the equilibrium on $N = \bar{N}$ for nominal values $M_{\text{fr}}(t) = \bar{M}_{\text{fr}}$, $M_{\text{pmp}}(t) = \bar{M}_{\text{pmp}}$, $M_L = \bar{M}_L$.

The linearized model of (12) can be approximated as in [16] for the air-bypass valve case, instead of electronic throttle

$$Y(s) = G_{\text{thr}}(s)e^{-st_d}U_1(s) + G_{\text{spk}}(s)e^{-st_{ds}}U_2(s) \quad (13)$$

where t_d is approximated as constant by computing (6) for $N(t) = \bar{N}$, and the output is the deviation of engine speed from idle speed setpoint, $y(t) = N(t) - \bar{N}$, in response to variations in the throttle position from nominal, $u_1(t) = \vartheta(t) - \bar{\vartheta}$, and to variations in the torque ratio from nominal, $u_2(t) = \kappa_{\text{spk}}(t) - \bar{\kappa}_{\text{spk}}$. In what follows, u_1, u_2 are also referred to as throttle (or airflow) input and spark input, respectively.

By (12) and the results in [16], the transfer functions in (13) are shown to be of the form

$$G_{\text{thr}}(s) = k_1 \frac{1}{\frac{s^2}{\omega_1^2} + 2\frac{\delta_1}{\omega_1}s + \omega_1^2} \quad (14a)$$

$$G_{\text{spk}}(s) = k_2 \frac{\frac{s}{a} + 1}{\frac{s^2}{\omega_2^2} + 2\frac{\delta_2}{\omega_2}s + \omega_2^2}. \quad (14b)$$

Model (14) is easily identifiable from both simulation and/or experimental data, for instance from step-response data. In particular, we can identify the linearized model from an available high-fidelity nonlinear simulation model based on (12). Even if direct identification from data is possible, we prefer to use a nonlinear simulation model first, because it allows us to evaluate the closed-loop behavior in simulation without the need of (cost and time) expensive data collection processes. Through simulations we obtain a feasibility assessment and a qualitative understanding of the effects of the tuning knobs on the closed-loop behavior more rapidly and systematically than possible by experiments. Through simulations we can verify the controller behavior even before the hardware is available and even against disturbances and uncertainties that are difficult to reproduce in vehicle tests.

The two transfer functions in (14) are converted to state space form and sampled with period $T_s = 30$ ms (roughly 10 times less than the plant time constant)

$$x_{\text{thr}}(k+1) = A_{\text{thr}}x_{\text{thr}}(k) + B_{\text{thr}}u_{\text{thr}}^\delta(k) \quad (15a)$$

$$y_{\text{thr}}(k) = C_{\text{thr}}x_{\text{thr}}(k) \quad (15b)$$

$$x_{\text{spk}}(k+1) = A_{\text{spk}}x_{\text{spk}}(k) + B_{\text{spk}}u_{\text{spk}}^\delta(k) \quad (16a)$$

$$y_{\text{spk}}(k) = C_{\text{spk}}x_{\text{spk}}(k) \quad (16b)$$

where $k \in \mathbb{Z}_{0+}$ is the sampling step $x_{\text{thr}}, x_{\text{spk}} \in \mathbb{R}^2$ and $u_{\text{spk}}^\delta, u_{\text{thr}}^\delta$ are the delay-free torque ratio and throttle command. For idle speed $\bar{N} = 600$ RPM, $t_d = 100$ ms $\approx 4T_s$. The discrete-time model of signal $u(\cdot)$ delayed by $n_\delta \in \mathbb{Z}_+$ steps is

$$x_\delta(k+1) = A_\delta x_\delta(k) + B_\delta u(k), \quad x_\delta \in \mathbb{R}^{n_\delta}$$

$$u_\delta(k) = C_\delta x_\delta(k)$$

$$A_\delta = \begin{bmatrix} 0 & \cdots & 0 \\ I_{n_\delta-1} & & \vdots \\ & & 0 \end{bmatrix}$$

$$B_\delta = [1 \ 0 \ \cdots \ 0]^T \\ C_\delta = [0 \ \cdots \ 0 \ 1]. \quad (17)$$

By cascading¹ a fourth-order airflow delay model (17) with (15), and a first-order spark delay model (17) with (16), we obtain the delayed dynamics

$$x_{\text{thr}}^f(k+1) = A_{\text{thr}}^f x_{\text{thr}}^f(k) + B_{\text{thr}}^f u_{\text{thr}}(k) \quad (18a)$$

$$y_{\text{thr}}^f(k) = C_{\text{thr}}^f x_{\text{thr}}^f(k) \quad (18b)$$

$$x_{\text{spk}}^f(k+1) = A_{\text{spk}}^f x_{\text{spk}}^f(k) + B_{\text{spk}}^f u_{\text{spk}}(k) \quad (19a)$$

$$y_{\text{spk}}^f(k) = C_{\text{spk}}^f x_{\text{spk}}^f(k) \quad (19b)$$

where $x_{\text{thr}}^f \in \mathbb{R}^6$, $x_{\text{spk}}^f \in \mathbb{R}^3$. Thus, the complete linear model of the engine is

$$x^p(k+1) = A^p x^p(k) + B^p u^p(k) \quad (20a)$$

$$y_p(k) = C^p x^p(k) \quad (20b)$$

$$x^p = \begin{bmatrix} x_{\text{thr}}^f \\ x_{\text{spk}}^f \end{bmatrix}, \quad u^p = \begin{bmatrix} u_{\text{thr}} \\ u_{\text{spk}} \end{bmatrix}, \quad A^p = \begin{bmatrix} A_{\text{thr}}^f & 0 \\ 0 & A_{\text{spk}}^f \end{bmatrix} \quad (20c)$$

$$B^p = \begin{bmatrix} B_{\text{thr}}^f \\ B_{\text{spk}}^f \end{bmatrix}, \quad C^p = [C_{\text{thr}}^f \quad C_{\text{spk}}^f] \quad (20d)$$

where $x^p \in \mathbb{R}^9$, and $u^p \in \mathbb{R}^2$.

Even though the main objective is the development of an MPC controller to coordinate the throttle and spark actuators, for comparison we have also designed another MPC controller that actuates only the throttle, while the conventional controller is retained to adjust the spark timing. For this single-input controller the plant model is obtained by removing G_{spk} from (13) and by repeating steps (15)–(20) to obtain the model

$$x^p(k+1) = A^p x^p(k) + B^p u^p(k) \quad (21a)$$

$$y_p(k) = C^p x^p(k) \quad (21b)$$

$$x^p = x_{\text{thr}}^f, \quad u^p = u_{\text{thr}}, \quad A^p = A_{\text{thr}}^f \quad (21c)$$

$$B^p = B_{\text{thr}}^f, \quad C^p = C_{\text{thr}}^f \quad (21d)$$

where now $x^p \in \mathbb{R}^6$, and $u^p \in \mathbb{R}$.

Remark 1: The physically actuated variable in (14b) is the spark ignition angle $\alpha(t)$, hence the nominal value of $\bar{\kappa}_{\text{spk}}$ is set by fixing a nominal value $\bar{\alpha}$, which is computed based on the nominal conditions at idle. Since α_{MBT} changes as operating conditions change [see (5)] while $\bar{\alpha}$ is basically kept constant, the range of u_2 (in particular the upper limit) will change. The limits on the torque ratio range will be introduced next, when discussing the constraints handled by the controller.

III. MPC DESIGN

MPC is a control strategy based on the receding horizon solution of a constrained finite horizon optimal control problem, formulated basing on a system prediction model, cost function and states, inputs, and outputs constraints. At every control cycle from the current state estimate, the finite horizon problem is

¹Although the delay occurs in the airflow dynamics, by model linearity it can be represented by an equivalent input delay.

solved, and the first element of the resulting optimal input sequence is applied to the system. At the following control cycle, the optimization is repeated starting from the newly estimated state and over a shifted horizon. We choose the controller sampling period $T_s = 30$ ms, consistently with the sampling period of the discrete-time models in Section II-A. This choice is also based on retaining the real-time task rate of the experimental platform, which is selected basing on a delicate tradeoff between performance and computational load.

The single-input and multi-input MPCs are designed from the prediction models derived in Section II-A. This process involves the augmentation of the model to enforce the specifications, the definition of the constraints and of the cost function, and the selection of the prediction, control and constraint horizons.

We begin with the throttle-only controller based on plant (21). In idle speed control, steady-state errors due to changes in load torque caused, for instance, by power steering or air-conditioning compressor, or due to errors in the scheduled airflow feedforward have to be removed. In order to achieve offset-free rejection of constant disturbances one can introduce *integral action* [28] by adding the dynamics

$$q_N(k+1) = q_N(k) + T_s(y_p(k) - r_{y_p}(k)) \quad (22)$$

where $q_N \in \mathbb{R}$ is the discrete-time integral of the output and $r_{y_p} \in \mathbb{R}$ is the desired idle speed set-point offset, where 0 offset corresponds to the nominal idle speed \bar{N} .

When (22) is added to (21), we obtain

$$x(k+1) = Ax(k) + Bu(k), \quad x = \begin{bmatrix} x_p \\ q_N \end{bmatrix}, \quad x \in \mathbb{R}^7 \quad (23a)$$

$$y(k) = Cx(k) \quad (23b)$$

$$A = \begin{bmatrix} A_p & 0 \\ T_s C_p & 1 \end{bmatrix}, \quad B = \begin{bmatrix} B_p \\ 0 \end{bmatrix}, \quad C = \begin{bmatrix} C_p & 0 \\ 0 & 1 \end{bmatrix}. \quad (23c)$$

which is the prediction model for the single-input controller.

Next, we define the constraints on system inputs and outputs. Limits on the engine speed, in r/min, are (conservatively) defined to avoid excessive engine flares and dips

$$-200 \leq y_p(k) - r_{y_p}(k) \leq 200. \quad (24)$$

In particular, avoiding large dips, especially below the so called fishhook point where engine friction increases dramatically, is critical for avoiding engine stalls. Additional limits on the throttle angle are imposed as

$$0 \leq u + u_{FF} \leq 10 \quad (25)$$

where $u_{FF}[\text{deg}]$ is the scheduled feedforward term in nominal conditions at idle, and ideally $u_{FF} = \bar{\vartheta}$, so that the feedforward term compensates for the nominal pumping and friction losses in (12b). The full (feedforward+feedback) throttle input is $\vartheta(t) = u_{FF} + u(t)[\text{deg}]$.

Finally, the cost function for the finite horizon optimal control problem in the MPC strategy is specified. Since a non-zero input

can be required at steady state to reject disturbances, we weigh the input increments in the cost function

$$\begin{aligned} J(\mathbf{y}(k), \mathbf{u}(k), u(k-1)) \\ = \sum_{i=0}^{h-1} (y(i|k) - r_y)^T Q (y(i|k) - r_y) + \Delta u(i|k) S \Delta u(i|k) \end{aligned} \quad (26)$$

where the notation $a(i|k)$ indicates the value of a predicted i steps ahead, from data at sampling instant k , $h \in \mathbb{Z}_+$ is the prediction horizon, $\mathbf{y}(k) = (y(0|k), \dots, y(h-1|k))$ and $\mathbf{u}(k) = (u(0|k), \dots, u(h-1|k))$ are the output and input sequences predicted at step k , respectively, $r_y = [r_{y_p} \ 0]^T$ is the output setpoint for the single-input controller, $\Delta u(i|k) = u(i|k) - u(i-1|k)$, and $u(-1|k) = u(k-1)$. Here, the weight matrices Q and S are assumed positive definite.

For the multi-input controller that actuates also the spark, additional requirements are imposed. The spark retard must return to its setpoint after disturbance rejection, for the controller to be able to counteract future disturbances. Hence, at steady state, the spark torque ratio must be at its nominal value ($u_2 = 0$), which requires an integrator on the torque ratio command to be weighed in the cost function

$$q_{\text{spk}}(k+1) = q_{\text{spk}}(k) + T_s u_2(k).$$

As a consequence, with A_p, B_p, C_p, x_p from (20), the prediction model used for controlling throttle and spark is

$$\begin{aligned} x(k+1) &= Ax(k) + Bu(k), \\ x &= \begin{bmatrix} x_p \\ q_N \\ q_{\text{spk}} \end{bmatrix}, \quad x \in \mathbb{R}^{11} \end{aligned} \quad (27a)$$

$$y(k) = Cx(k) \quad (27b)$$

$$A = \begin{bmatrix} A_p & 0 & 0 \\ T_s C_p & 1 & 0 \\ 0 & 0 & 1 \end{bmatrix}, \quad B = \begin{bmatrix} B_p \\ 0 & 0 \\ 0 & T_s \end{bmatrix},$$

$$C = \begin{bmatrix} C_p & 0 & 0 \\ 0 & 1 & 0 \\ 0 & 0 & 1 \end{bmatrix}. \quad (27c)$$

The spark ignition angle range is limited, and as a consequence the torque ratio is constrained. The lower bound of u_2 depends on the engine and aftertreatment operating conditions, but it is kept constant for simplicity since it is generally not reached unless during very short transients. The upper bound varies since α_{MBT} changes while $\bar{\alpha}$ is kept constant, for ECU functional reasons. Hence, the constraint

$$-0.1 \leq u_2(k) \leq \Delta \kappa_{\text{spk}}^{\text{max}}(k) \quad (28)$$

needs to be enforced, the upper bound, $\Delta \kappa_{\text{spk}}^{\text{max}}(k)$, being a non-linear function of engine speed, load, and temperature. We represent $\Delta \kappa_{\text{spk}}^{\text{max}}(k)$ as a parameter whose current value is known, and which is assumed constant over the controller prediction horizon. For the multi-input controller, cost function (26) is still used, with different sizes for the weighting matrices and

$r_y = [r_{y_p} \ 0 \ 0]^T$. Combining (23)–(26) for the throttle controller, or (24)–(28) for the throttle and spark controller, we formulate the MPC finite horizon optimal control problem

$$\min_{\sigma, \mathbf{u}(k)} \quad \rho \sigma^2 + \sum_{i=0}^{h-1} (y(i|k) - r_y)^T Q (y(i|k) - r_y) + \Delta u(i|k)^T S \Delta u(i|k) \quad (29a)$$

$$\text{s.t.} \quad x(i+1|k) = Ax(i|k) + Bu(i|k), \quad (29b)$$

$$y(i|k) = Cx(i|k), \quad i = 0, \dots, h-1 \quad (29c)$$

$$u_{\min} \leq u(i|k) \leq u_{\max}, \quad i = 0, \dots, h_u - 1 \quad (29d)$$

$$y_{\min} - \sigma \mathbf{1} \leq y(i|k) \leq y_{\max} + \sigma \mathbf{1}, \quad i = 1, \dots, h_c \quad (29e)$$

$$u(i|k) = u(h_u - 1|k), \quad i = h_u, \dots, h-1 \quad (29f)$$

$$\sigma \geq 0 \quad (29g)$$

$$u(-1|k) = u(k-1), \quad x(0|k) = x(k) \quad (29h)$$

where $\mathbf{1}$ is a vector of 1 of appropriate dimensions, $x(k)$ is the state (estimate) at time k , h is the prediction horizon, $h_c \leq h$ is the constraint horizon, and $h_u \leq h$ is the control horizon. The output constraints (29e) are “softened” by the additional optimization variable $\sigma \in \mathbb{R}$ to avoid a situation where (29) becomes unfeasible (e.g., due to large unmeasured disturbances) and no control action is computed since no solution to the finite horizon optimal control problem exists. Soft constraints violation results in a large penalty, modelled by weighting σ in the cost function by $\rho > 0$, with ρ at least two orders of magnitude larger than the other weights.

For the single-input idle speed MPC controller, in (29)

$$\begin{aligned} y_{\min} &= \begin{bmatrix} -200 + r_{y_p}(k) \\ -\infty \end{bmatrix} \\ u_{\min} &= -u_{FF} \\ y_{\max} &= \begin{bmatrix} 200 + r_{y_p}(k) \\ +\infty \end{bmatrix} \\ u_{\max} &= 10 - u_{FF} \end{aligned}$$

while for the multiple input idle MPC controller

$$\begin{aligned} y_{\min} &= \begin{bmatrix} -200 + r_{y_p}(k) \\ -\infty \\ -\infty \end{bmatrix}, \quad u_{\min} = \begin{bmatrix} -u_{FF} \\ -0.1 \end{bmatrix} \\ y_{\max} &= \begin{bmatrix} 200 + r_{y_p}(k) \\ +\infty \\ +\infty \end{bmatrix}, \quad u_{\max} = \begin{bmatrix} 10 - u_{FF} \\ \Delta \kappa_{\text{spk}}^{\max}(k) \end{bmatrix}. \end{aligned}$$

The current values of $\Delta \kappa_{\text{spk}}^{\max}(k)$ and $r_{y_p}(k)$ are computed by the software running in the vehicle ECU.

Remark 2: $\Delta \kappa_{\text{spk}}^{\max}(k)$ has effect on the input constraints, while $r_y(k)$ has effect on the output constraints and on the cost function. Both $\Delta \kappa_{\text{spk}}^{\max}(k)$ and $r_y(k)$ are parameters of the optimization problem. Their current values are known and they are assumed constant over the prediction horizon.

Recall that the basic model predictive control algorithm executes the following steps, at each control cycle $k \in \mathbb{Z}_{0+}$: (i) from available measurements, the state estimate $x(k)$ is computed; (ii) the quadratic programming problem (29) is solved,

obtaining the optimal input sequence $\mathbf{u}^*(k)$; (iii) the first element of the optimal input sequence is applied to the plant as current input $u(k) = u^*(0|k)$.

Since only the engine speed is measured, a state estimator is required for step (i). For the idle speed controllers, a stationary Kalman filter has been used for estimating x^p

$$x^p(k|k-1) = A^p x^p(k-1) + B^p u^p(k-1) \quad (30a)$$

$$x^p(k) = x^p(k|k-1) + K_{KF}(y_p(k) - C^p x^p(k|k-1)) \quad (30b)$$

where K_{KF} is the stationary Kalman filter gain $K_{KF} = PC^p T (C^p PC^p T + R_{KF})^{-1}$ and P is the solution of the algebraic Riccati equation $P = A^p P A^p T + Q_{KF} - A^p PC^p T (C^p PC^p T + R_{KF})^{-1} C^p P A^p T$. Kalman filter (30) is tuned by Q_{KF} and R_{KF} , that represent process and measurement noise covariances, respectively, and set the tradeoff between convergence speed and noise rejection.

Remark 3: We have used integral action to achieve offset-free constant disturbance rejection. An alternative approach is to use a disturbance model [29], where the prediction model is augmented by an output additive disturbance state, modelled by integrated white noise and estimated via the Kalman filter. However, in early development phases we have found that in ISC the resulting system is poorly observable and the Kalman filter is extremely sensitive to the tuning parameters. Hence, for ISC application we have found integral action simpler to calibrate.

The controller is tuned by selecting the cost function weights in (26), and possibly the Kalman filter covariances in (30). When control horizon and constraint horizon are considered, the prediction horizon h is a tuning parameter that does not affect the number of constraints, and hence the complexity of the control-law, but cost function (26), and hence the closed-loop performance and stability, only. In general, h shall be chosen to cover the significant components of the transients, hence of the same order of magnitude than the plant time constant.

A. Closed-Loop Simulations

The two MPC controllers are tested in closed loop with a nonlinear simulation model based on (12), and where the parameters are identified from experimental data as polynomials of the engine operating conditions, namely engine load and speed. The parameters in (14) are obtained by step response on each channel (throttle angle and torque ratio). The evolution of the engine speed as predicted by the linearized model $\hat{N}(t) = y_p(t) + \bar{N}$, $\bar{N} = 600$ r/min is compared to the engine speed evolution for the nonlinear model, $N(t)$, in Fig. 2. The plot of the error $\varepsilon_N(t) = \hat{N}(t) - N(t)$ indicates a satisfactory fit. The controllers are implemented with $h = 30$, $h_c = 3$, $h_u = 3$ in (29).

We have considered a simulated test in which the controller has to reject a torque disturbance representing a load change, caused for instance by power steering, transmission engagement, or air-conditioning compressor activation. The additional load is engaged and maintained for several seconds, then released. In these simulations, a load of 20 Nm is used. The main performance measure of this test is the maximum deviation of the engine speed from idle. In particular, a large dip following an increased load may cause the engine to stall, and hence it

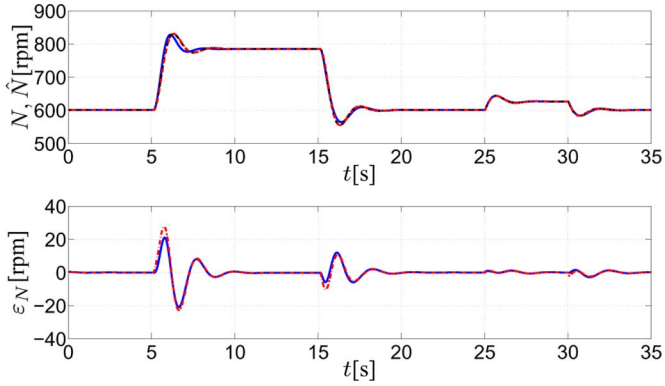


Fig. 2. Validation of the ISC plant model identified from simulation data. Upper plot: nonlinear model (dashed line), continuous-time linearized model (solid line), discrete-time linearized model (dashed-dotted line). Lower plot: difference between continuous-time linearized model and nonlinear model (solid line) and between discrete-time linearized model and nonlinear model (dashed-dotted line).

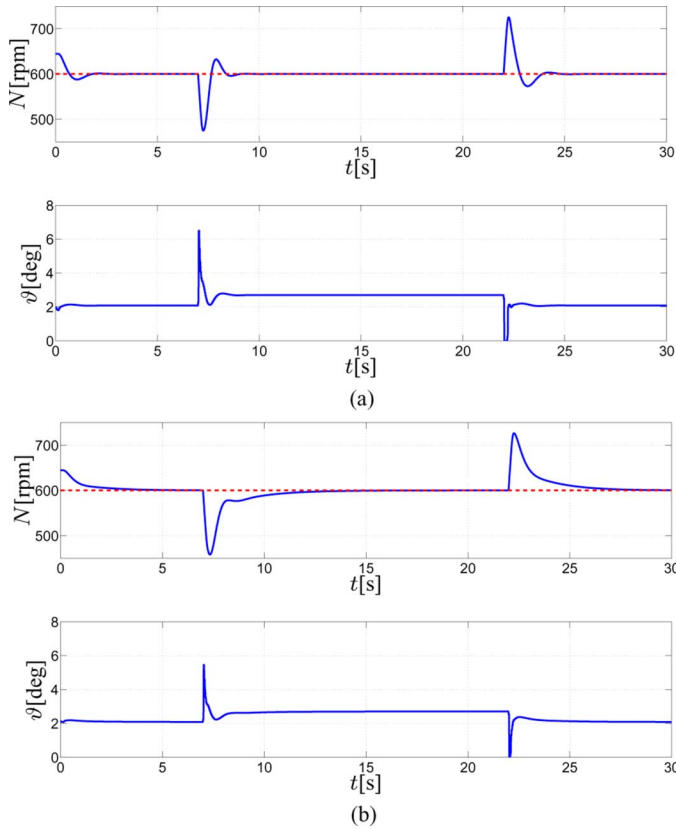


Fig. 3. Simulation of the single-input MPC idle speed controller in closed-loop with the nonlinear engine model. (a) Underdamped closed-loop dynamics. (b) Overdamped closed-loop dynamics.

is considered the most critical performance parameter. A large flare, in the case of a reduction in the load, is also undesirable for both fuel economy and noise, even though not as critical. An additional performance parameter is the settling time to the set-point.

The single-input MPC controller problem (29) is defined using the identified parameters within (23). Simulation results for the single-input controller in a disturbance rejection test are shown in Fig. 3. In this test the spark retard was kept constant at

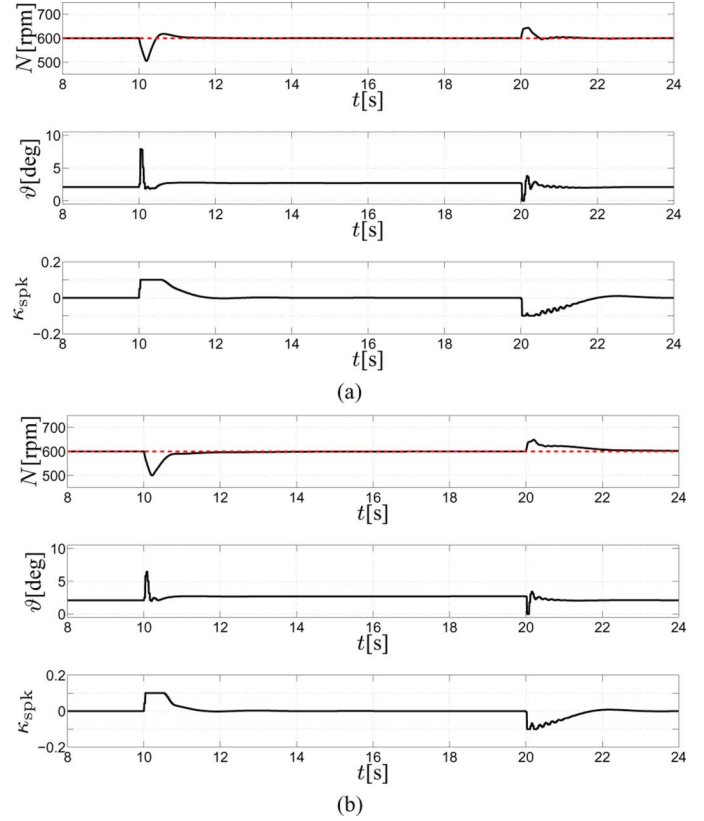


Fig. 4. Simulation of the multiple-input MPC idle speed controller in closed-loop with the nonlinear engine model. (a) Underdamped closed-loop dynamics. (b) Overdamped closed-loop dynamics.

its nominal value and the throttle was the only available degree of freedom for the controller.

Fig. 3 shows the results obtained for different tunings of the engine speed tracking error weight. In Fig. 3(a) a more aggressive tuning [achieved by reducing S in (29)] is used, so that the controller is faster in rejecting the disturbances, but exhibits an underdamped behavior, while in Fig. 3(b) a slower overdamped behavior is achieved. The knowledge acquired in the simulation phase on how the parameters of the cost function affect the closed-loop behavior (which is nonlinear and difficult to predict) is valuable in speeding up the controller calibration during real experiments.

The simulation results for the multi-input MPC controller based on prediction model (27) with the identified parameters for the same disturbances amplitude are shown in Fig. 4, where once again two closed-loop behaviors are reported. Only a part of the simulation is shown to improve readability of the results. Since the nonlinear simulation model does not represent the variation of the available torque ratio due to α_{MBT} variations, $\Delta \kappa_{\text{spk}}^{\text{max}}(k)$ is assumed constant. Note that, in both cases the controllers achieve better disturbance rejection compared to the corresponding single-input MPC in terms of maximum deviation from the setpoint and settling time.

IV. CONTROLLER SYNTHESIS AND ANALYSIS

The simulation results of Section III-A indicate that satisfactory performance can be achieved. However, before proceeding

to experiments, three more steps are required. First, the controller complexity must be evaluated and proved computationally feasible in the automotive ECU. Second, the asymptotic stability of the closed-loop should be assessed. Finally, the prediction model should be refined using experimental data from the test vehicle. For instance, in our case the simulation model introduced in Section III-A was made available to us prior to the availability of the experimental vehicle, and that model was parameterized for a different vehicle.

A. Feedback Law Synthesis and Functional Assessment

Solving the optimal control problem (29) in conventional automotive microcontrollers may be too demanding from a computational viewpoint. Also, the CPU operations and the memory requirements of the optimization algorithms are difficult to predict. To overcome these difficulties, the MPC controller is explicitly synthesized [14]. Due to the input rate cost term, the explicit MPC control law (the first element of the solution of (29)) is a piecewise affine function of the current state $x = x(k)$, reference² $r = \begin{bmatrix} r_y^T(k) \Delta \kappa_{\text{spk}}^{\max}(k) \end{bmatrix}^T \in \mathbb{R}^{n_r}$, and of the past input $u_{-1} = u(k-1)$

$$u(k) = \varphi_{\text{MPC}}(x, r, u_{-1}) \quad (31a)$$

$$\varphi_{\text{MPC}}(x, r, u_{-1}) = F_i^x x + F_i^r r + F_i^u u_{-1} + g_i \quad (31b)$$

$$i \in \{1, \dots, s\} : H_i^x x + H_i^r r + H_i^u u_{-1} \leq \mathcal{K}_i \quad (31c)$$

where (31c) defines a polyhedral partition of the state-reference-past input space and s is the number of regions. Hence, for any $i \in \{1, \dots, s\}$, (31b) defines the polyhedron $\mathcal{P}_i = \{(x, r, u_{-1}) \in \mathbb{R}^{n_x+n_r+n_u} : H_i^x x + H_i^r r + H_i^u u_{-1} \leq \mathcal{K}_i\}$ and for any $i, j \in \{1, \dots, s\}$, $i \neq j$, $\text{int}(\mathcal{P}_i) \cap \text{int}(\mathcal{P}_j) = \emptyset$, where $\text{int}(\cdot)$ indicates the interior of a set. Once the explicit MPC law (31) is synthesized, the control algorithm is as follows. At time k :

- (i) from the measurement $y(k)$ and previous state estimate $x(k-1)$, compute the state estimate $x(k)$ by the Kalman filter (30);
- (ii) search for $\bar{i} \in \{1, \dots, s\}$ such that (31c) is satisfied for $x(k)$, $r(k)$, $u(k-1)$;
- (iii) evaluate (31b) for $i = \bar{i}$ to compute $u(k)$;
- (iv) apply $u(k)$.

In order to compute the explicit MPC law, the evaluation of scalar sums, products, and comparisons is required, only. The most computationally demanding step is to search for the currently active region [step (ii)] that requires the evaluation of several linear inequalities. After the region is found, only one instance of (31b) is evaluated to compute the control input.

Even though a precise and tight bound on the number of regions is difficult to provide *a priori* [14], since a region represents an active set of constraints, the number of regions is bounded by the number of combinations of constraints in the optimization problem [14], and their dimension is the sum of the state, input, and reference vector dimensions. Thus, the constraint and control horizons may need to be changed to reduce

²The measured limit $\Delta \kappa_{\text{spk}}^{\max}$ is added to the reference vector, since it does not change over the prediction horizon.

the complexity of the explicit control law, if this is dictated by the available computational power. For the idle speed control optimization problem (29), $h = 30$, $h_c = 3$, $h_u = 3$. Thus, for the single-input controller there are six input constraints and six output constraints enforced along the horizon. The obtained explicit controller is composed of 35 regions, and the parameters in function $\varphi_{\text{MPC}}(\cdot)$ are seven states, two references, one previous input. The worst case number of operations for both region search and command computation that have to be executed at each control cycle is less than 5000, which amounts to less than $2 \cdot 10^5$ operations per second. The data memory usage is less than 3 kB. For the multi-input controller with the same values of h, h_c, h_u , the complexity is higher because of the additional constraints on the torque ratio and the higher dimension of the prediction model. As a result, the explicit controller is composed of 131 regions, and, since there are now 11 components in the state vector, 2 in the previous input vector, and 4 references³, the maximum number of operations per control cycle is always less than $45 \cdot 10^3$, implying a maximum of $1.5 \cdot 10^6$ operations per second. The data memory usage for the controller is less than 50 kB. Note that the computed CPU load represents a conservative upper bound, while the average CPU load is significantly less.

According to the projections in [30], the explicit controller uses less than 0.05% of the CPU in the worst case for the single-input controller, and less than 1.5% for the multi-input controller. It shall be noted that at idle the microcontroller is, in general, underloaded, due to the low rate of engine event triggered tasks, which is a reflection of the low engine speed. Furthermore, the memory occupancy for the single-input and multi-input controller are in the order of 0.15% and 2.5% of the available memory, respectively. Further complexity reduction can be obtained by the techniques surveyed in [31], which however are not needed here.

B. Closed-Loop Analysis

Contrary to infinite horizon linear quadratic regulators (LQR), asymptotic stability is not guaranteed for model predictive controllers. Stability can be guaranteed *a priori* by adding terminal state or terminal set constraints, and by possibly modifying the cost function [32]. However, the terminal constraint requires in general long horizons to be satisfied, and as a consequence the complexity of the explicit MPC law may grow too large for automotive applications. A different approach is to enforce a control Lyapunov function [32] by an additional set of constraints, but also in this case the complexity of the explicit MPC law is increased and the recursive feasibility [i.e., the continued existence of solution of (29)] may not be guaranteed.

Thus, MPC designs with *a priori* stability guarantee may be either conservative or impractical for fast automotive applications. At the same time, once the explicit MPC law is computed, stability can still be checked *a posteriori*. The closed-loop dynamics where the plant is controlled by (31) are described by

³For simplicity all the references are considered as variable parameters. The references on the integral actions can be fixed to 0 to reduce the number of parameters. The bound on the torque ratio has been accounted for in the reference vector.

TABLE I

NUMERICAL RESULTS OF MINIMUM, MAXIMUM, AND RMS OF THE ERROR SIGNAL (e) ON THE POWERSTEERING DISTURBANCE REJECTION TEST (PS), AND IN THE DOUBLE DISTURBANCE REJECTION (DD) TEST. BASELINE CONTROLLER (BASE), SINGLE-INPUT MPC (SI-MPC), MULTI-INPUT MPC (MI-MPC), MULTI-INPUT MPC WITH REDUCED RESERVE (MRD-MPC)

Controller	PS, min(e)	PS, max(e)	PS, rms(e)	DD, min(e)	DD, max(e)	DD, rms(e)
Base	-172.96	134.42	13.82	-280.62	208.50	29.16
si-MPC	-97.57	88.48	7.03	-216.81	132.46	11.67
mi-MPC	-82.76	86.34	6.00	-118.60	104.56	8.92
mrd-MPC	-116.55	118.91	8.43	-189.28	136.99	12.93

a piecewise affine (PWA) dynamical system [33]. Let us define the closed-loop system state

$$\chi(k) = \begin{bmatrix} x(k) \\ u(k-1) \end{bmatrix}$$

then the closed-loop dynamics are

$$\chi(k+1) = \begin{bmatrix} A^p + B^p F_i^x & B F_i^u \\ F_i^x & F_i^u \end{bmatrix} \chi(k) + \begin{bmatrix} B F_i^r \\ F_i^r \end{bmatrix} r(k) + \begin{bmatrix} B \\ I \end{bmatrix} g_i \quad (32a)$$

$$i \in \{1, \dots, s\} : [H_i^x \quad H_i^u] \chi(k) + H_i^y r(k) \leq \mathcal{K}_i. \quad (32b)$$

If there exists a quadratic or a piecewise quadratic Lyapunov function for (32), (semi)global asymptotic stability is verified [34]. The existence of such functions can be proven by solving linear matrix inequalities (LMIs). While quadratic Lyapunov functions may be conservative, resulting in overconstrained LMIs often infeasible, piecewise quadratic Lyapunov functions require the solution of LMIs whose complexity grows with the number of regions, and hence may become hard to solve for PWA systems with many regions. Besides global analysis, a local stability analysis of (32) can be easily performed. Let $\bar{\chi}$ be the equilibrium corresponding to nominal idle speed and the nominal reference \bar{r} , i.e., engine speed and setpoint at nominal idle, nominal idle load, and spark and throttle at nominal values, and let \bar{i} be the index of region $\mathcal{P}_{\bar{i}}$ such that $(\bar{\chi}, \bar{r}) \in \mathcal{P}_{\bar{i}}$. For correctly chosen nominal idle conditions, $(\bar{\chi}, \bar{r}) \in \text{int}(\mathcal{P}_{\bar{i}})$, and $g_{\bar{i}} = 0$. Thus, in a region around $\bar{\chi}$ the dynamics are defined by (32), where $i = \bar{i}$, and the local stability analysis reduces to the one of a linear system. It is also important to note that the region of attraction of the stable equilibrium contains at least [35] the set $(\mathcal{X} \times \{\bar{r}\}) \subseteq \mathcal{P}_{\bar{i}}$, where \mathcal{X} is the largest positive invariant set [36] contained in $\mathcal{P}_{\bar{i}}$ when $r = \bar{r}$ for the closed-loop dynamics (32), where $i = \bar{i}$. By the technique described above, for the single-input controller providing underdamped closed-loop response in the simulations of Section III-A, we obtain the spectral radius⁴ of the closed-loop state transfer matrix $\rho = 0.845$ while for the corresponding multi-input controller is $\rho = 0.815$. Such an approach can be used also to analyze the stability margins, and as a consequence the parametric robustness of the closed-loop system.

⁴The spectral radius is defined as the maximum of the magnitude of the eigenvalues λ_i of the state transfer matrix, i.e., $\rho = \max_i |\lambda_i|$. For linear discrete-time systems, $\rho < 1$ implies asymptotic stability.

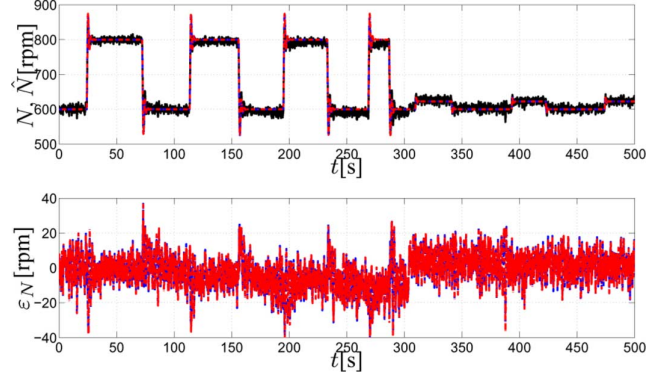


Fig. 5. Validation of the ISC plant model identified from experimental data. Upper plot: experimental data (solid line), continuous-time linearized model (dashed line), discrete-time linearized model (dashed-dotted line). Lower plot: difference between continuous-time linearized model and experimental data (solid line) and between discrete-time linearized model and experimental data (dashed-dotted line).

Remark 4: The assumption $(\bar{\chi}, \bar{r}) \in \text{int}(\mathcal{P}_{\bar{i}})$ is justified by the fact that the PWA regions are defined by the active constraints sets. As a consequence, the borders of the regions are the boundaries where the active set changes. It is a reasonable assumption that, in a set of conditions around nominal idle, neither the output, nor the input constraints are active. Hence $(\bar{\chi}, \bar{r}) \in \text{int}(\mathcal{P}_{\bar{i}})$. Similar reasons justify the assumption $g_{\bar{i}} = 0$, in nominal conditions.

C. Prediction Model Refinement

With controller design, synthesis, analysis, and computational feasibility assessment now complete, we proceed with the controller development based on the experimental data and in the experimental vehicle. The results of the identification based on the experimental data from a 4.6 L, V8 engine are shown in Fig. 5, where the identified engine model is validated with respect to the experimental data in throttle step response tests. The model error is larger than the one in Fig. 2. However, since MPC is a feedback strategy, it can handle well this model uncertainty. The experimental data can be used to evaluate the measurements and process noise, and the modeling errors. This allows improved tuning of the Kalman filter (30). Once the physical model is updated, the explicit MPC controllers can be synthesized again and the stability analysis of Section IV-B can be repeated. By changing the prediction model, the cost function weights may need to be updated as well. The knowledge achieved by the closed-loop simulations of Section IV-A and automated procedures (e.g., [35]) indicate how to update the cost function weights to achieve the desired closed-loop behavior.

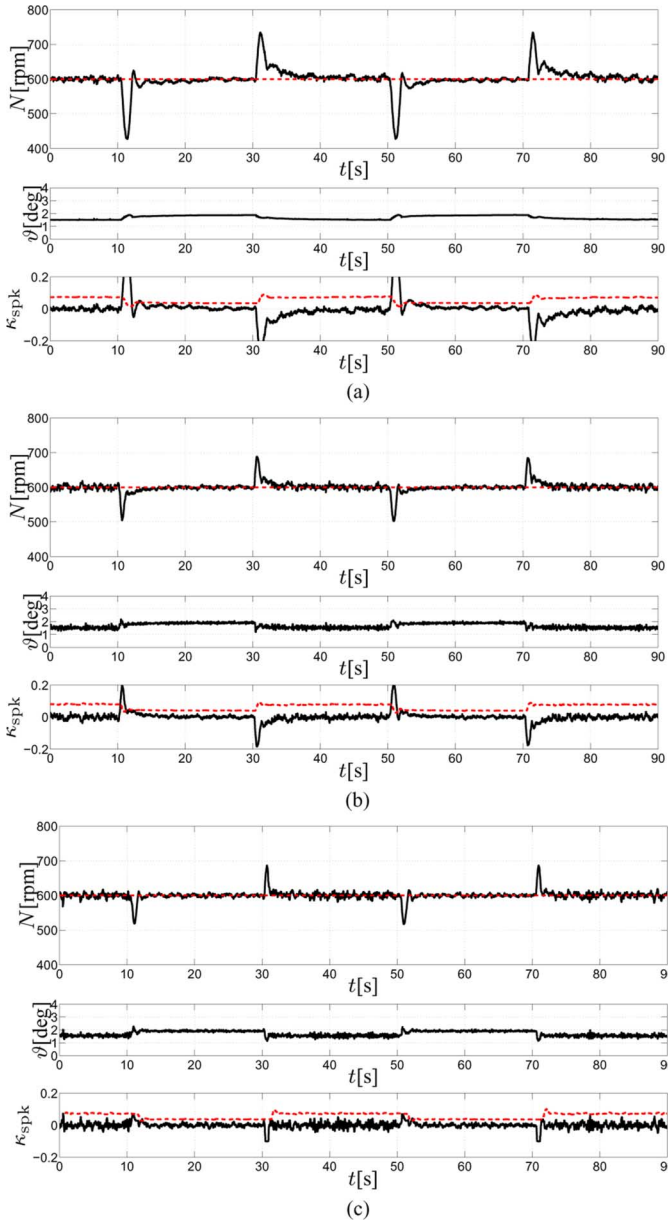


Fig. 6. Power steering disturbance rejection test. Closed-loop response of the different controllers. (a) Base controller. (b) Single-input MPC controller. (c) Multi-input MPC controller.

V. EXPERIMENTAL RESULTS

The controllers designed in Section III are tested on a fully functional production vehicle equipped with the 4.6L V8 engine, whose dynamics have been identified in Section IV-C, with an electronic throttle, and a 4 gear automatic transmission. For speeding up the calibration process, the controllers are implemented in a dSPACE MicroAutoBox rapid prototyping unit, which communicates with the powertrain ECU via CAN protocol. During the experiments, the MPC controller runs in parallel to the standard ECU software. In details, the ECU provides the engine speed measurements used in the Kalman filter (30) to the MPC controller and, by estimating the current MBT ignition angle (5), the torque ratio limits (28). The ECU also converts the torque ratio in a spark ignition angle by inverting (4), and provides the low-level interface with the actuators, by issuing the

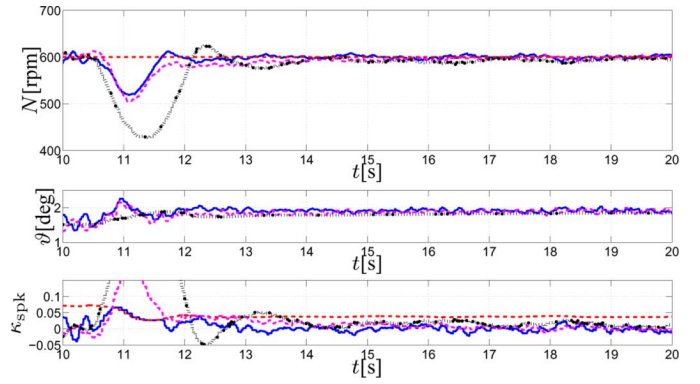


Fig. 7. Comparison in power steering disturbance rejection test. Base controller (dotted line), single-input MPC (dashed line), multi-input MPC (solid line).

ISC command to the actuators drivers every 30 ms. Even if it is executed in a separated computing unit, the explicit MPC is coded in ANSI C, and it is compatible with the code running in the standard ECU. The communication via CAN induces a delay in the data exchange between ECU and MPC controller. This delay, in the order of 10 ms, is limited when compared to the controller sampling period, however it still slightly penalizes the prototype MPC controller versus a realization in the ECU.

The MPC controllers are compared with a baseline controller, which is an error-based feedback controller actuating throttle and spark torque ratio independently basing on engine speed measurement, with built-in nonlinearities that counteract particularly critical situations. The base controller structure is depicted in Fig. 1(b). The spark controller is of proportional-derivative (PD) type and the throttle controller is of proportional-integral (PI) type. The commands are saturated *a posteriori* in the admissible range, and a classical anti-windup scheme [37] is implemented in the PI channel. The base controller has been independently tuned to provide a good tradeoff between performance and robustness throughout all the test conditions, and the performance limitations are mainly due to input saturations and to the plant time-delay.

The single-input MPC controller overrides the PI channel only, while it keeps the base spark controller, including the *a-posteriori* command saturation. The multi-input MPC controller overrides both channels, hence achieving better coordination between the two actuators.

Several experimental tests have been performed in different conditions, see Table I for a summary of the results. As mentioned before, the most critical performance parameter is the size of the “dip” in the engine speed following a disturbance.

In Fig. 6 we present a disturbance rejection test where the power steering is engaged at maximum power (by pushing the steering wheel at the end of its travel with the cutoff switch disabled) and then disengaged, twice. This causes step changes of about 22 Nm in the load on the crankshaft, which are larger than the disturbances encountered in normal conditions. No information about the load changes is available to the controller, hence the load is entirely rejected by feedback control. The power steering is first engaged at $t = 10$ s, released at $t = 30$ s, then engaged again at $t = 50$ s and released at $t = 70$ s. The performance of the base controller is shown in Fig. 6(a). In Fig. 6(b),

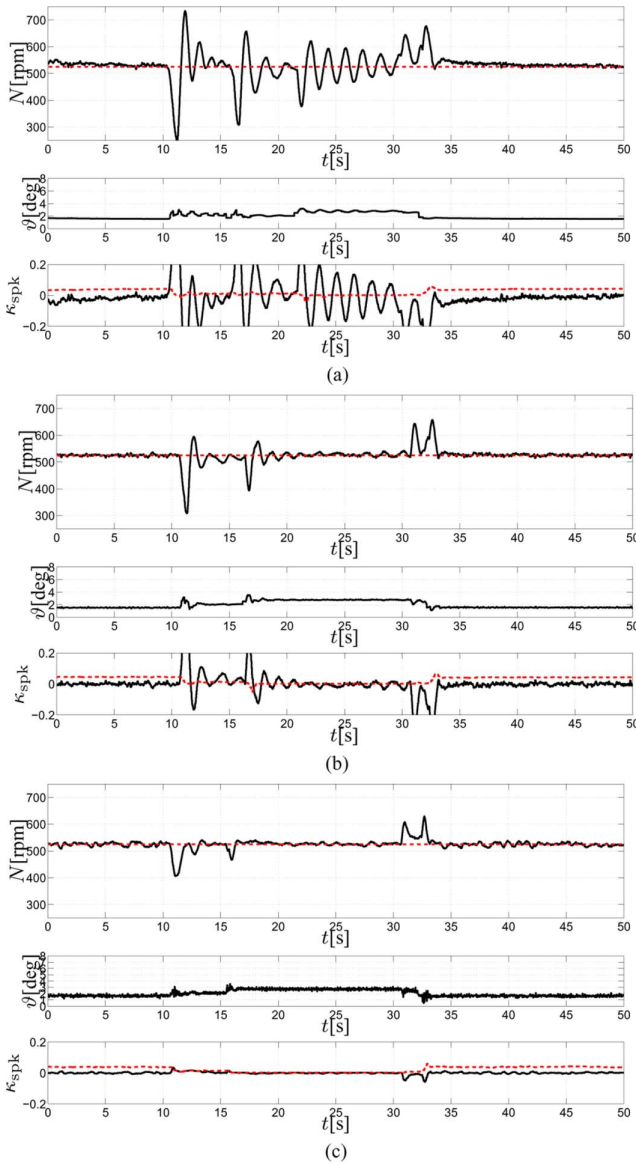


Fig. 8. Double disturbance rejection test. Closed-loop response of the different controllers. (a) Base controller. (b) Single-input MPC. (c) Multi-input MPC.

the response of the single-input MPC is shown, where a noticeable improvement in disturbance rejection and tracking performance can be seen. This is to a significant extent due to the use of the prediction model to account for the time lag in the manifold dynamics and for the torque production delay, which allows one to increase the feedback action without losing stability. Furthermore, the MPC controller is a (nonlinear) state feedback that selects a control strategy, rather than a single control input, based on its prediction model and accounting for the system constraints. Thus, additional degrees of freedoms can be exploited to achieve higher performance. However, one can see that the torque ratio command still does not comply with the available torque ratio reserve (dashed line in the lowest plot), which means that it is saturated *a posteriori*, and not delivered. As a consequence, we expect that the performance can be further improved by the multi-input MPC controller which accounts for the available torque reserve. The performance of

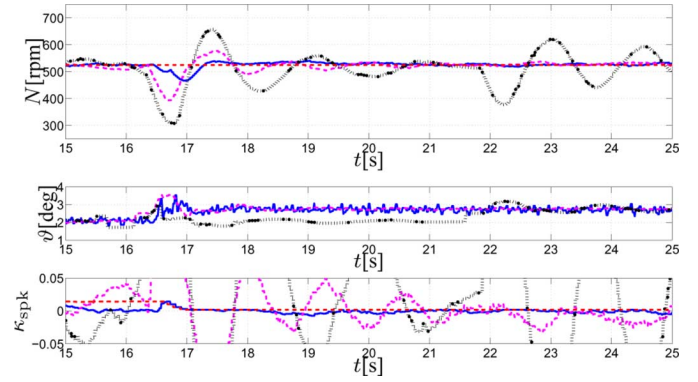


Fig. 9. Comparison in double disturbance rejection tests. Base controller (dotted line), single-input MPC (dashed line), multi-input MPC (solid line).

that is shown in Fig. 6(c). Note that the requested torque ratio constraint is now enforced⁵ (the maximum available $\Delta\kappa_{\text{spk}}^{\text{max}}$ is shown by the dash line) and, as a result, the disturbance rejection and tracking performance are further improved. A comparison of the performance of the three controllers in rejecting the first power steering disturbance is shown in Fig. 7.

A more challenging test is shown in Fig. 8, where, with the gear in drive, the power steering is engaged at full power at $t = 10$ s, and the air conditioning compressor is engaged at full power at $t = 15$ s, then both of them are disengaged at $t = 30$ s. The air conditioning compressor causes an additional 16 Nm load on the crankshaft. Indeed, the total disturbance is much larger than the disturbances that occur in normal conditions [25]. When in drive, the nominal idle speed is $\bar{N} = 525$ RPM, slightly lower than when in neutral, causing a longer delay (6).

The test shows that the advantage of the MPC controllers is not only the reduction of the engine speed error after a disturbance, but also faster setpoint tracking. When multiple disturbances hit in sequence, fast convergence to the setpoint after each disturbance is important for maintaining disturbance rejection capabilities with respect to subsequent disturbances.

The performance of the base controller is shown in Fig. 8(a). When the second disturbance hits, at around 15 s, the engine speed is still far from the setpoint. Also, due to the increased load, a reduced torque ratio from the spark is available, which causes larger effects from the *a posteriori* saturation. The result is a significantly reduced performance. The single-input MPC, see Fig. 8(b), still presents the problem of neglecting torque ratio saturation, but thanks to the improved performance of the throttle control, the closed-loop behavior is certainly improved. In this test a major advantage is obtained by the multi-input MPC controller [see Fig. 8(c)], which is aware of the reduced spark authority, and can coordinate the two actuators. The controller acts more aggressively on the throttle, to compensate for the reduced spark authority.

A closer, comparative view of the rejection of the second disturbance, the engagement of the AC compressor, is shown in Fig. 9, where the time axis of the different experiments have been slightly realigned for better comparison.

⁵The torque ratio upper bound signal is recorded at a slightly lower rate. Hence, the small violations in Fig. 7 are only apparent, due to the logging process.

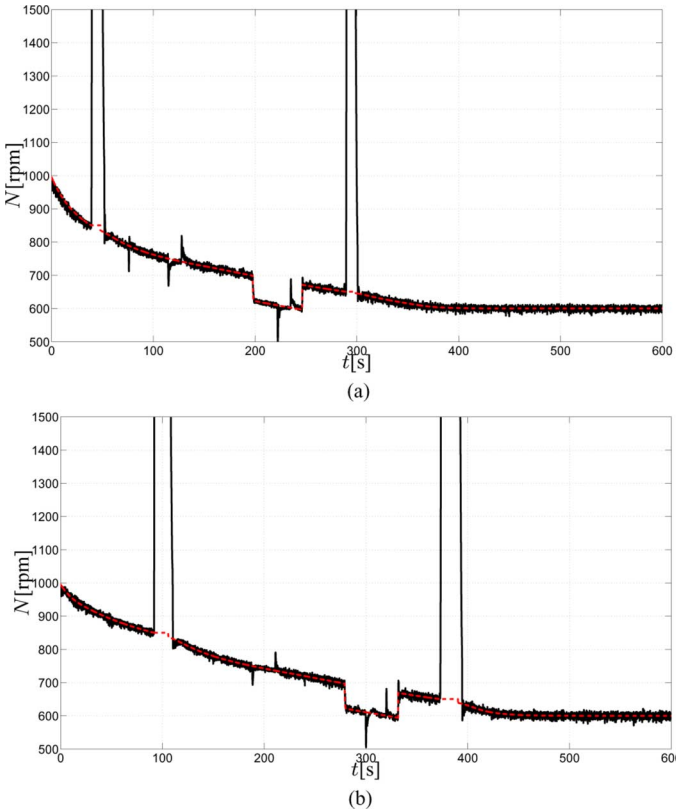


Fig. 10. MPC controllers behavior during cold start subject to several different disturbances. (a) Single-input MPC. (b) Multi-input MPC.

In Fig. 10 we show the behavior of the single-input and multi-input MPC controllers when operating in non-nominal conditions, namely in cold start conditions. See Fig. 10(a) and (b), respectively. In this case the idle setpoint starts from about 1000 RPM and decreases, while the engine is warming up from approximately 60 F to the nominal operating engine coolant temperature of 192 F. Several disturbances are introduced during the tests, including power steering engagement/disengagement, shifts between neutral and drive (indicated by sharp drops/increases in the setpoint, see Fig. 10(a) at around 200 and 250 s, and Fig. 10(b) at around 280 and 330 s), tip-in/tip-out (indicated by the engine speed that suddenly ramps to large values, then quickly decreases to idle again). The response to a tip-out is particularly critical because the idle controller is disengaged until the engine speed is around idle, and it needs to act quickly, in order to reduce the engine speed deceleration and to avoid the engine speed to drop too much below the setpoint, that may stall the engine. Fig. 10 shows that both the MPC controllers can perfectly deal with a plant in non-nominal conditions.

Finally, we show that thanks to the improved controller performance, it is possible to reduce the spark reserve at idle, thus improving fuel economy. In details, we have modified the ECU configuration so that the spark nominal ignition angle $\bar{\alpha}$ is 5 degrees closer to nominal MBT, and as a consequence, the maximum available torque ratio is reduced. Since the spark setpoint is closer to the maximum efficiency value, this spark reserve reduction translates in approximately a 6.5% improved fuel economy while idling in neutral, and approximately 4.5% while idling in drive.

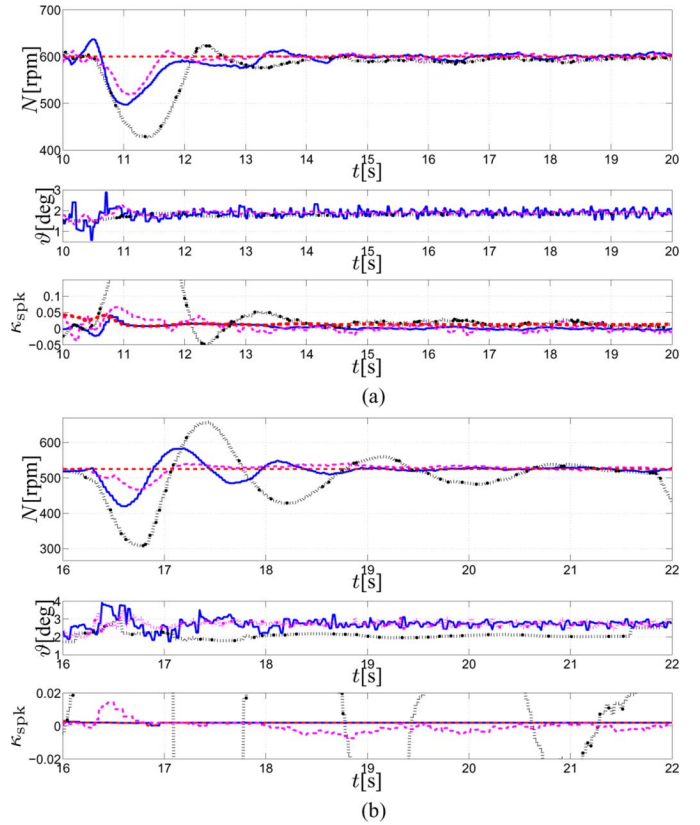


Fig. 11. Performance of the multi-input MPC controller with reduced spark reserve. Multi-input MPC with reduced reserve (solid line), multi-input MPC with full reserve (dashed line), base controller with full reserve (dotted line). (a) Comparison in the power steering disturbance rejection test. (b) Comparison in the double disturbance rejection test.

We have repeated the test scenarios of Fig. 6–10. Due to space limitations, we do not report the complete experiments, but only a comparison of the controllers in Fig. 11. In Fig. 11(a), we compare the drop caused by the disturbance generated by power steering motor engagement, similar to Fig. 7. The response of the multi-input MPC with reduced reserve (solid line), the multi-input MPC with full reserve (dashed line), and the base controller with full reserve (dotted line) are shown. Although the performance of the MPC with reduced reserve is slightly worse than the one of the MPC with full reserve, due to reduced spark actuation authority, the performance is still better than the one of the base controller. For the double disturbance test, similarly to what is shown in Fig. 9, the response at the engagement of the second disturbance (A/C compressor), while the power steering motor is at saturation of the steering wheel range, is shown in Fig. 11(b). Once again, the MPC with reduced reserve is slightly worse than the one with full reserve, but significantly outperforms the base controller. Note that the controller reacts to the reduced available spark reserve by a stronger action of the throttle.

Table I summarizes the results of the experiments, by presenting a set of performance criteria computed on the error signal $e(k) = y(k) - r_y(k)$ for the different controllers. The performance criteria are the minimum $\min(e) = \min_{k=1, \dots, N_{\text{sim}}} e(k)$, the largest engine speed “dip”, the maximum, $\max(e) = \max_{k=1, \dots, N_{\text{sim}}} e(k)$, the largest

engine speed “flare”, and the root mean square error, $\text{rms}(e) = \sqrt{1/N_{\text{sim}} \sum_{k=1}^{N_{\text{sim}}} e(k)^2}$, where N_{sim} is the duration of the experiments in steps. For the MPC controller with reduced reserve, the performance is still better than the base controller, even though it is worse than the MPC with full reserve, due to reduced authority of the fast actuator, the spark timing.

It is worth to point out that during the executed tests, the average CPU load is less than 10% the worst case computed in Section IV-A. The reason is that most of the active controller regions are found rapidly, because of the region search order. This can be further improved by choosing an “optimal” region ordering or using advanced search techniques [38]. Furthermore, for a non-active region, as soon as one violated constraint is found, the algorithm moves to evaluate the next region, hence several constraints do not need to be evaluated. However, when dimensioning a real-time controller, the worst-case CPU load is the parameter to consider, since the algorithm must always have the time to execute completely.

VI. CONCLUSION

We have presented the development, implementation, analysis, and experimental evaluation of model predictive controllers for idle speed control. The overall procedure has been formalized in a design process flow that aims at minimizing the development time and effort, by appropriately using simulation models, controller analysis tools, and experimental data, and by focusing at each step on the meaningful tuning parameters.

For idle speed control, we have shown improved performance and robustness of the MPC controllers compared to existing controllers in an experimental vehicle. We attribute these improvements to MPC taking into account the effects of the delay, thanks to the prediction model, the constraints on the actuators, and, in the multi-input controller case, the coordination between throttle angle and spark timing. Our results have also demonstrated that MPC implementation of the idle speed controller is computationally feasible in production ECUs, and that because of the improved disturbance rejection capabilities, engine calibrations that provide improved fuel economy may become feasible.

ACKNOWLEDGMENT

The authors would like to thank J. Doering, Ford Research and Advanced Engineering, for valuable discussions and suggestions on spark actuation and testing procedures.

REFERENCES

- [1] S. Di Cairano, D. Yanakiev, A. Bemporad, I. Kolmanovsky, and D. Hrovat, “An MPC design flow for automotive control and applications to idle speed regulation,” in *Proc. 47th IEEE Conf. Dec. Control*, 2008, pp. 5686–5691.
- [2] S. Di Cairano, D. Yanakiev, A. Bemporad, I. Kolmanovsky, and D. Hrovat, “Model predictive powertrain control: An application to idle speed regulation,” *Lecture Notes Control Inf. Sci.*, no. 402, pp. 183–194, 2010.
- [3] C. Garcia, D. Prett, and M. Morari, “Model predictive control: Theory and practice—a survey,” *Automatica (Oxford)*, vol. 25, no. 3, pp. 335–348, 1989.
- [4] J. Rawlings and D. Mayne, *Model Predictive Control: Theory and Design*. Madison, WI: Nob Hill Publishing, LLC, 2002.
- [5] P. Ortner and L. del Re, “Predictive control of a diesel engine air path,” *IEEE Trans. Control Syst. Technol.*, vol. 15, no. 3, pp. 449–456, May 2007.
- [6] G. Stewart and F. Borrelli, “A model predictive control framework for industrial turbodiesel engine control,” in *Proc. 47th IEEE Conf. Dec. Control*, Dec. 2008, pp. 5704–5711.
- [7] R. Schalllock, K. Muske, and J. P. Jones, “Model predictive functional control for an automotive three-way catalyst,” *SAE Int. J. Fuels Lubricants*, vol. 2, no. 1, pp. 242–249, 2009.
- [8] S. Trimboli, S. Di Cairano, A. Bemporad, and I. Kolmanovsky, “Model predictive control for automotive time-delay processes: An application to air-to-fuel ratio,” in *Proc. 8th IFAC Workshop Time-Delay Syst.*, 2009, pp. 1–6.
- [9] R. Amari, M. Alamir, and P. Tona, “Unified MPC strategy for idle-speed control, vehicle start-up and gearing applied to an automated manual transmission,” in *Proc. 17th IFAC World Congr.*, 2008, pp. 7079–7085.
- [10] S. Di Cairano, A. Bemporad, I. Kolmanovsky, and D. Hrovat, “Model predictive control of magnetically actuated mass spring dampers for automotive applications,” *Int. J. Control*, vol. 80, no. 11, pp. 1701–1716, 2007.
- [11] A. Grancharova and T. Johansen, “Explicit model predictive control of an electropneumatic clutch actuator using on/off valves and pulsewidth modulation,” in *Proc. Eur. Control Conf.*, 2009, pp. 1–6.
- [12] G. Ripaccioli, A. Bemporad, F. Assadian, C. Dextreit, S. Di Cairano, and I. Kolmanovsky, “Hybrid modeling, identification, and predictive control: An application to hybrid electric vehicle energy management,” in *Hybrid Systems: Computation and Control*, ser. Lecture Notes in Computer Science. New York: Springer, 2009, vol. 5469, pp. 321–335.
- [13] H. Borhan, C. Zhang, A. Vahidi, A. Phillips, M. Kuang, and S. Di Cairano, “Predictive energy management of a power-split hybrid electric vehicle,” in *Proc. 49th IEEE Conf. Dec. Control*, 2010, pp. 4890–4895.
- [14] A. Bemporad, M. Morari, V. Dua, and E. Pistikopoulos, “The explicit linear quadratic regulator for constrained systems,” *Automatica*, vol. 38, no. 1, pp. 3–20, 2002.
- [15] L. Guzzella and C. Onder, *Introduction to Modeling and Control of Internal Combustion Engine Systems*. New York: Springer, 2004.
- [16] D. Hrovat and J. Sun, “Models and control methodologies for IC engine idle speed control design,” *Control Eng. Pract.*, vol. 5, no. 8, pp. 1093–1100, 1997.
- [17] A. Stotsky, B. Egardt, and S. Eriksson, “Variable structure control of engine idle speed with estimation of unmeasurable disturbances,” *ASME J. Dyn. Syst., Meas., Control*, vol. 122, pp. 599–603, 2000.
- [18] D. Hrovat, “MPC-based idle speed control for IC engine,” presented at the FISITA Conf., Prague, Czech Republic, 1996.
- [19] C. Carnevale and A. Moschetti, “Idle speed control with H -infinity technique,” presented at the SAE World Congr., Detroit, MI, 1993.
- [20] D. Hrovat and B. Bodenheimer, “Robust automotive idle speed control design based on μ -synthesis,” in *Proc. Amer. Control Conf.*, Jun. 1993, pp. 1778–1783.
- [21] G. Puskorius, L. Feldkamp, and L. Davis, “Dynamic neural network methods applied to on-vehicle idle speed control,” *Proc. IEEE*, vol. 84, no. 10, pp. 1407–1420, Oct. 1996.
- [22] K. Butts, N. Sivasankar, and J. Sun, “Application of ℓ_1 optimal control to the engine idle speed control problem,” *IEEE Trans. Autom. Control*, vol. 7, no. 2, pp. 258–270, Feb. 1999.
- [23] S. Benghea, X. Li, and R. De Carlo, “Combined controller-observer design for uncertain time delay systems with applications to engine idle speed control,” *J. Dyn. Syst., Meas. Control*, vol. 126, pp. 772–780, 2004.
- [24] L. Glielmo, S. Santini, and I. Cascella, “Idle speed control through output feedback stabilization for finite time delay systems,” in *Proc. Amer. Control Conf.*, 2000, pp. 45–49.
- [25] X. Li and S. Yurkovich, “Sliding mode control of delayed systems with application to engine idle speed control,” *IEEE Trans. Control Syst. Technol.*, vol. 9, no. 6, pp. 802–810, Nov. 2001.
- [26] Y. Yildiz, A. Annaswamy, D. Yanakiev, and I. Kolmanovsky, “Adaptive idle speed control for internal combustion engines,” in *Proc. Amer. Control Conf.*, 2007, pp. 3700–3705.
- [27] J. Deur, S. Magner, M. Jankovic, and D. Hrovat, “Influence of intake manifold heat transfer effects on accuracy of SI engine air charge prediction,” presented at the ASME Int. Mech. Eng. Congr. Expo., Anaheim, CA, 2004.

- [28] H. Kwakernaak and R. Sivan, *Linear Optimal Control Systems*. New York: Wiley-Interscience, 1972.
- [29] G. Pannocchia and J. Rawlings, "Disturbance models for offset-free model-predictive control," *AIChE J.*, vol. 49, no. 2, pp. 426–437, 2003.
- [30] S. Magner, S. Cooper, and M. Jankovic, "Engine control for multiple combustion optimization devices," presented at the SAE World Congr., Detroit, MI, 2006.
- [31] A. Alessio and A. Bemporad, "A survey on explicit model predictive control," in *Nonlinear Model Predictive Control: Towards New Challenging Applications*, ser. Lecture Notes in Control and Inf. Sciences. Berlin Heidelberg, Germany: Springer, 2009, vol. 384, pp. 345–369.
- [32] D. Mayne, J. Rawlings, C. Rao, and P. Scokaert, "Constrained model predictive control: Stability and optimality," *Automatica*, vol. 36, no. 6, pp. 789–814, Jun. 2000.
- [33] A. Bemporad, W. Heemels, and B. De Schutter, "On hybrid systems and closed-loop MPC systems," *IEEE Trans. Autom. Control*, vol. 47, no. 5, pp. 863–869, May 2002.
- [34] G. Ferrari-Trecate, F. Cuzzola, D. Mignone, and M. Morari, "Analysis of discrete-time piecewise affine and hybrid systems," *Automatica*, vol. 38, pp. 2139–2146, 2002.
- [35] S. Di Cairano and A. Bemporad, "Model predictive control tuning by controller matching," *IEEE Trans. Autom. Control*, vol. 55, no. 1, pp. 185–190, Jan. 2010.
- [36] E. Gilbert and K. T. Tan, "Linear systems with state and control constraints: The theory and applications of maximal output admissible sets," *IEEE Trans. Autom. Control*, vol. 36, no. 9, pp. 1008–1020, Sep. 1991.
- [37] K. Åström and B. Wittenmark, *Computer Controlled Systems*. Englewood Cliffs, NJ: Prentice-Hall, 1984.
- [38] P. Tøndel, T. Johansen, and A. Bemporad, "Evaluation of piecewise affine control via binary search tree," *Automatica*, vol. 39, no. 5, pp. 945–950, 2003.



Stefano Di Cairano (M'08) received the Master's degree in computer engineering and the Ph.D. degree in information engineering from the University of Siena, Siena, Italy, in 2004 and 2008, respectively.

In 2008, he was granted the International Curriculum Option for Doctoral Studies in hybrid control for complex distributed and heterogeneous embedded systems. In 2002–2003, he was Visiting Student at the Technical University of Denmark, Lyngby, Denmark. In 2006–2007, he was Visiting Researcher at the Control and Dynamical Systems

Department, the California Institute of Technology, Pasadena, CA, where he joined the team competing in the 2007 DARPA Urban Challenge. In 2008, he joined Powertrain Control Research and Advanced Engineering Department, Ford Motor Company, Dearborn, MI, where he is now a Technical Expert. His research focuses on the application of optimization-based control algorithms to complex systems including powertrain, vehicle dynamics, energy management, and supply chains. His research interests include automotive control, model predictive control, networked distributed control systems, hybrid systems, optimization algorithms, and stochastic control.



Diana Yanakiev (M'07) received the diploma from Technical University of Sofia, Bulgaria, in 1989, and the M. S. and Ph.D. degrees in electrical engineering (control systems) from the University of California, Los Angeles, in 1994 and 1997, respectively.

The topic of her graduate research was longitudinal control of heavy-duty vehicles on automated highway systems. From 1997 to 2001, she worked with Cummins Engine Company in the areas of engine testing automation and diesel engine control. She joined Ford Motor Company, Dearborn, MI,

in 2001, where she has worked on control of hybrid vehicles, spark-ignition internal combustion engines, and automatic transmissions.



Alberto Bemporad (F'10) received the Master's degree in electrical engineering and the Ph.D. degree in control engineering from the University of Florence, Florence, Italy, in 1993 and 1997, respectively.

He spent the academic year 1996/1997 at the Center for Robotics and Automation, Department of Systems Science and Mathematics, Washington University, St. Louis, as a Visiting Researcher. In 1997–1999, he held a postdoctoral position at the Automatic Control Laboratory, ETH, Zurich, Switzerland, where he collaborated as a Senior Researcher in 2000–2002. In 1999–2009, he was with the Department of Information Engineering of the University of Siena, Italy, becoming an Associate Professor in 2005. Since 2010, he has been with the Department of Mechanical and Structural Engineering, University of Trento, Trento, Italy. He has published over 220 papers in the areas of model predictive control, hybrid systems, automotive control, multiparametric optimization, computational geometry, robotics, and finance. He is coauthor of the *Model Predictive Control Toolbox* (The Mathworks, Inc., 1998) and author of the *Hybrid Toolbox for MATLAB* (2003).

Dr. Bemporad was an Associate Editor of the IEEE TRANSACTIONS ON AUTOMATIC CONTROL during 2001–2004. He is Chair of the Technical Committee on Hybrid Systems of the IEEE Control Systems Society since 2002.



Ilya Kolmanovsky (F'08) received the M.S. and Ph.D. degrees in aerospace engineering, and the M.A. degree in mathematics from the University of Michigan, Ann Arbor, in 1993, 1995, and 1995, respectively.

Before becoming a Professor with the Department of Aerospace Engineering, University of Michigan, in 2010, he was with Ford Motor Company for close to 15 years. He has published over 200 refereed journal and conference articles on a spectrum of theoretical topics, and on a variety of automotive and aerospace control applications. He holds 82 U.S. patents.

Dr. Kolmanovsky was a recipient of several awards, including Donald P. Eckman Award of American Automatic Control Council, of IEEE Transactions on Control Systems Technology Outstanding Paper Award and of several innovation and technical achievement awards at Ford Motor Company. He is a member of IEEE Control Systems Society Board of Governors.



Davor Hrovat (F'07) received the B.Sc. M.E. (Dipl. Ing.) degree from the University of Zagreb, Croatia, in 1972, and the M.Sc. and Ph.D. degrees in mechanical engineering from the University of California, Davis, in 1976 and 1979, respectively.

Since 1981, he has been with the Ford Research Laboratory (FRL), Dearborn, MI, where he is a Henry Ford Technical Fellow, coordinating and leading research efforts on various aspects of vehicle/power train control systems. He holds numerous U.S. patents.

Dr. Hrovat has served on editorial boards for a number of ASME and IEEE journals, and is currently an Editor for the IFAC journal *Control Engineering Practice* and the *International Journal of Vehicle Autonomous Systems*. He is a Fellow of the American Society of Mechanical Engineers (ASME). He was a recipient of the 1996 ASME/Dynamic Systems and Control Innovative Practice Award and the 1999 AACC Control Engineering Practice Award. He is a member of the National Academy of Engineering.